Australian Winter Mountain Storm Clouds: Precipitation Augmentation Potential

ALEXIS B. LONG

Division of Atmospheric Research, CSIRO, Aspendale, Victoria, Australia and Desert Research Institute, Atmospheric Sciences Center, Reno, Nevada

ELIZABETH J. CARTER

Desert Research Institute, Atmospheric Sciences Center, Reno, Nevada

(Manuscript received 3 September 1994, in final form 24 April 1995)

ABSTRACT

Two Australian winter mountain storm field research projects were conducted by the Commonwealth Scientific and Industrial Research Organisation Division of Atmospheric Research and the Desert Research Institute Atmospheric Sciences Center in the austral winters of 1988 and 1990. These projects gained information about winter storms in support of the ongoing Melbourne Water randomized cloud seeding experiment aimed at increasing runoff into Melbourne's main water supply, the Thomson Reservoir. This paper discusses some of the 1988 instrumentation data. One variable of interest is the precipitation augmentation potential π. It is the difference between (a) the horizontal supercooled liquid water flux in the clouds crossing the mountains and (b) the vertical precipitation flux at the surface from the clouds. These fluxes are based on calculations of supercooled liquid water depth in clouds with a microwave radiometer, Omegasonde wind velocity, and rates of precipitation from gauges. It was found that π varies systematically during a winter storm. The greatest potential occurs in the post-cold-frontal stage of a storm when the cloud-top temperature is warm and about -12°C and the wind direction of 240° is approximately orthogonal to the main southwest face of the predominant orographic feature, Baw Baw Plateau, of the study area. The potential is significantly less during the prefrontal and frontal stages, with cloud-top temperatures of about -35°C and a wind direction of about 300° parallel to the Baw Baw Plateau. The results show that cloud seeding would have the greatest benefit in the postfrontal stage.

1. Introduction

The Melbourne and Metropolitan Board of Works, now known as Melbourne Water, conducted a randomized, cloud seeding, precipitation augmentation experiment from 1988 to 1992. It was aimed at enhancing the precipitation over the catchment of the Thomson Reservoir, which is Melbourne's main water supply. During two years of the experiment, 1988 and 1990, a field research study was conducted of clouds and precipitation in the experimental area. This study was a joint exercise of the Commonwealth Scientific and Industrial Research Organisation (CSIRO) Division of Atmospheric Research and the Desert Research Institute (DRI) Atmospheric Sciences Center. The aim of the study was to understand the circumstances under which several water substance variables, including the precipitation augmentation potential, would be significant.

As will be seen, the potential depends partly upon the supercooled liquid water in the clouds in the study area. It is worthwhile noting a few earlier findings about the supercooled liquid water that are relevant to the present study. Cooper and Saunders (1980) and Marwitz (1986) observed with sondes and aircraft that the greatest supercooled liquid water in winter storms in the San Juan Mountains in southwestern Colorado occurs in a convectively unstable stage late in the history of a storm. Heggli and Rauber (1988) found that in a significant number of synoptic storms the supercooled liquid water was greatest in the postfrontal orographic parts of synoptic storms. Significant supercooled liquid water associated with mesoscale bands of synoptic systems was observed (Hobbs 1978), especially with bands ascending rising terrain.

In every synoptic or mesoscale situation noted above there is significant atmospheric lift. The lift promotes the condensation of water substance from the vapor. If the temperature is less than 0°C, then the condensed water substance may be supercooled liquid.

The supercooled liquid water has two overriding effects. First, it provides an environment for the nucleation of ice particles and then for the growth of those particles, initially by deposition and eventually by accretion. Second, the growth induces an increasing particle terminal fall velocity, which influences the trajec-

Corresponding author address: Dr. Alexis B. Long, 144 Jasper Road, Bentleigh, Victoria 3204, Australia.

tory taken by the particle. This trajectory may terminate at the ground or the particle may sublimate or evaporate into the air.

The object of cloud seeding is to place artificial ice nuclei in a region of supercooled liquid water such that ice particles may grow to precipitable sizes and such that the acquired trajectories may carry the particles to a desired ground target area. It should be noted that the volume occupied by the supercooled liquid water must be large enough that when filled with artificial ice nuclei a useful mass of additional precipitation will eventually reach the ground.

2. Instrumentation

The full complement of data sources including instrumentation were synoptic data including surface and upper-level maps, Japanese Geostationary Meteorological Satellite visible and infrared cloud imagery, Omegasondes, a microwave radiometer, surface precipitation microphysics observations, and a precipitation gauge network. Some of these data sources, highlighted below, provided the information used in the present paper. Figure 1 shows the research study area as well as the seeding experiment target and control areas. Additional information on the instrumentation and its assumptions and accuracy is available in Long and Huggins (1992) and is not repeated here.

a. Omegasondes

Vaisala/Digi-Cora Omegasondes were launched by the Bureau of Meteorology personnel at Blue Rock Reservoir, shown in Fig. 1. Launches were made every 3 or 6 h during winter storms that passed through the experimental area. The typical sonde collected data up to the 120-hPa level. The variables sampled were equivalent potential temperature, temperature, dewpoint temperature, and wind speed and direction.

b. Radiometer

The Desert Research Institute operated its microwave radiometer (see Hogg et al. 1983) on Baw Baw Plateau, shown in Fig. 1. The radiometer was pointed toward the zenith and measured the line integral (depths are in millimeters through the cloud) of liquid water passing overhead every 2 min.

c. Precipitation gauge network

Altogether, 87 precipitation gauges were placed in the experimental area (see Fig. 1). The gauges were of the tipping-bucket kind with digital data logging. The gauges were 95% reliable and temporally accurate to ±2 min. The precipitation that entered a gauge was known to within 2%.

3. Definitions of water substance variables

The instrumentation placed in the field allowed the measurement of a number of water substance variables and calculation of others, all related to the opportunities for precipitation augmentation.

Figure 2 is a schematic cross section through Baw Baw Plateau (1500 m MSL), the Melbourne Water (MW) Thomson Reservoir (500 m MSL), and hills to the east. It shows a schematic trajectory of an Omegasonde launched upwind of the plateau, the locations of precipitation gauges on the plateau, and the location of the radiometer. The two large arrows represent E and P, as discussed below.

a. Calculations of water substance fluxes E and P

The horizontal supercooled liquid water flux comes from the formula

$$E\,(\mathrm{ML\ h^{-1}}) = 3.6W\,(\mathrm{mm})\bar{V}(\mathrm{m\ s^{-1}})\bar{d}(\mathrm{km}). \quad (1)$$

In this equation, W is the supercooled liquid water depth measured with the radiometer, $\bar{V}$ is the mean Omegasonde wind speed in the cloud layer estimated to contain the supercooled liquid water, and $\bar{d}$ is the mean crosswind dimension of the target area as viewed downwind. All of these quantities and E are calculated every 15 min. Details of this equation, including an error analysis, appear in Long and Huggins (1992). The numerical factor 3.6 converts the units on the right-hand side of (1) to the units on the left-hand side.

The vertical precipitation flux comes from the formula

$$P\,(\mathrm{ML\ h^{-1}}) = \frac{1}{10}\sum_{i=1}^{10} r_i\,(\mathrm{mm\ h^{-1}})\,A\,(\mathrm{km^2}), \quad (2)$$

where r_i is the precipitation rate at the surface at the ith of the 10 gauges in the target area. The area A of the target area is 487 km^2. An average precipitation of 1 mm melted depth over the target area amounts to 487 ML. Equation (2) is also discussed in Long and Huggins (1992).

b. Precipitation augmentation potential π

The precipitation augmentation potential π is the amount (ML h^{-1}) by which the precipitation could be augmented by seeding on the basis of using all or part of E. Here, π is bounded as follows:

$$E - P \leq \pi \leq E, \quad E \geq P, \quad (3a)$$

$$0 \leq \pi \leq E, \quad E \leq P, \quad (3b)$$

or

$$\max(E - P, 0) \leq \pi \leq E. \quad (3c)$$

The lower and upper bounds on π are known as π_l and π_u, respectively.

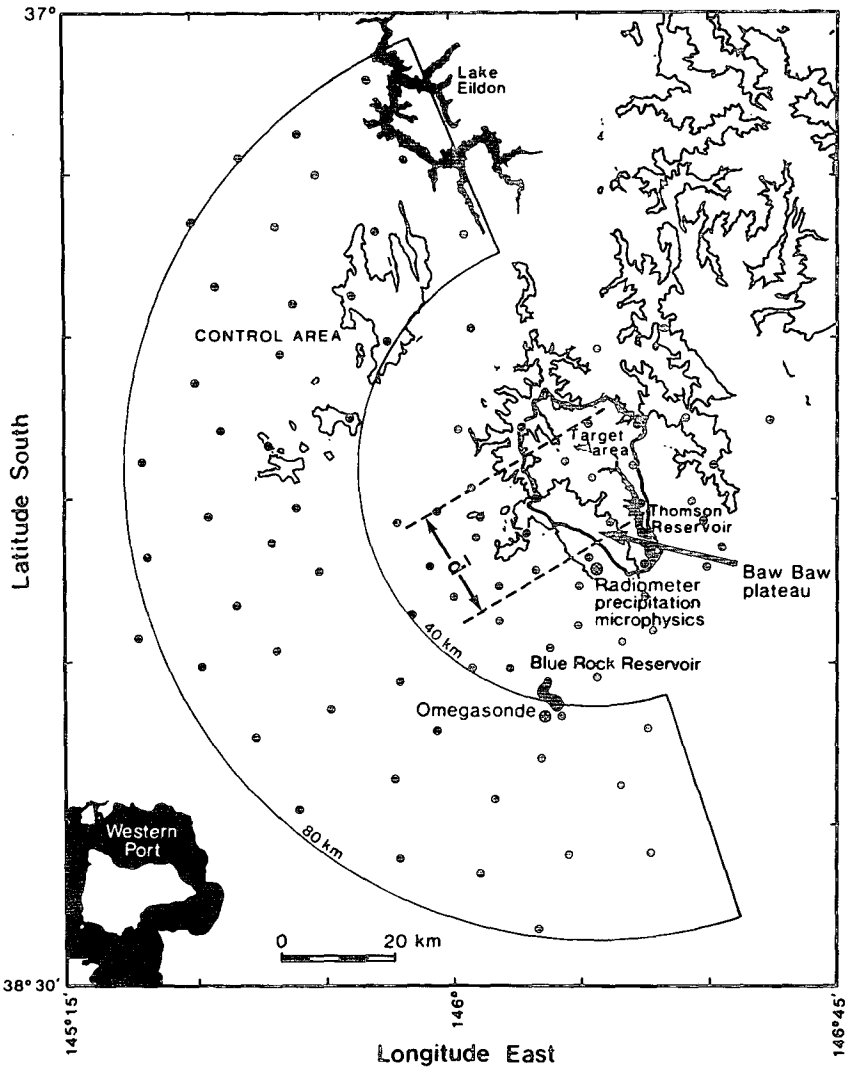

FIG. 1. Map of the target and control areas of the Melbourne Water cloud seeding experiment. The 1988 research study collected data at the sites shown, including the solid circles (precipitation gauges). The present research is concerned with (a) the horizontal supercooled liquid water flux E across the southwestern, western, and northwestern borders of the target and (b) the downwind precipitation flux P in the target area. The contour interval is at 1000 m MSL.

If $E \geq P$ [Eq. (3a)], the lower bound on π assumes that E contributed (a) to downwind precipitation flux P first and foremost and that (b) only the positive excess supercooled liquid water flux in the amount $E - P$ can be identified with precipitation augmentation potential that could be realized by cloud seeding activities. The upper bound on π assumes that (a) E does not contribute to downwind precipitation flux P at all and that (b) all supercooled liquid water flux in the amount E can be identified with precipitation augmentation potential that could be realized by cloud seeding activities.

If $E \leq P$ [Eq. (3b)], the lower bound on π assumes that all of E contributes to downwind precipitation flux P. The upper bound on π assumes that (a) E does not contribute to downwind precipitation flux P at all and that (b) all supercooled liquid water flux in the amount E can be identified with precipitation augmentation potential that could be realized by cloud seeding activities.

Previous treatments (Long and Huggins 1992; Heggli 1986; Boe and Super 1986; Rauber and Grant 1987; Super and Boe 1988) have acknowledged the upper bounds E on π but have not considered the lower bounds treated here. These lower bounds represent a *conservative* assumption about the least amount of su-

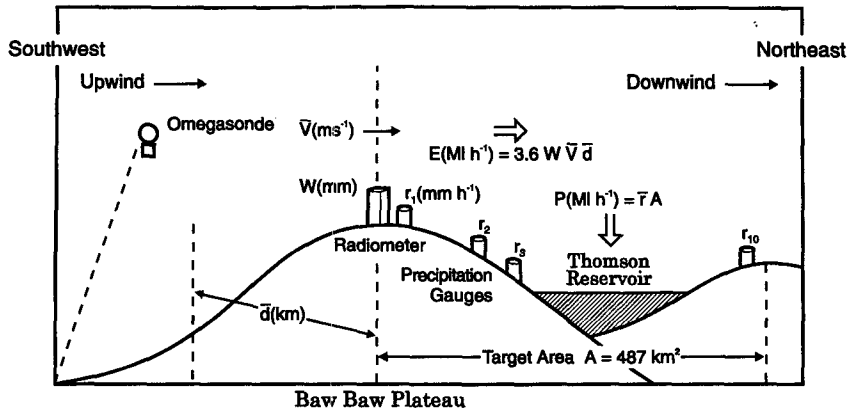

FIG. 2. Schematic diagram of locations of instrumentation on Baw Baw Plateau and of fluxes E and P and other variables discussed in the text.

percooled liquid water flux that is available for cloud seeding activities.

It should be noted that limited artificial ice nucleation rates, limited particle growth rates within the supercooled liquid water from deposition or accretion, fall trajectories not terminating in a desired target area, and low below-cloud humidities are all factors that could reduce the actual flux of surface precipitation, due to augmentation activities, below the positive values within the inequalities in (3). These factors, which could reduce augmented precipitation, could be the subject of future research.

c. *Timescales ratio* ρ

The quotient of (1) divided by (2) yields

$$\rho = \frac{E}{P} = \left(\frac{W}{\bar{r}}\right)\left(\frac{3.6\bar{V}\bar{d}}{A}\right) = \left(\frac{T_a}{T_b}\right), \qquad (4)$$

where the time $T_a = W/\bar{r}$ and T_b equals the other term. The times T_a and T_b have the following definitions: T_a—minimum time (h) for complete consumption of the supercooled liquid water as precipitation, and T_b—time (h) required for the supercooled liquid water to move across the target area. Combining these definitions yields the following interpretation for ρ, namely, that $\rho = T_a/T_b$ is the minimum time needed to consume by precipitation the supercooled liquid water as it moves over the target area divided by the time required for the air containing the evolving supercooled liquid water to move across the target area.

If $T_a \leq T_b$, then $\rho \leq 1$, and natural precipitation processes can be said to be fast. All supercooled liquid water is potentially consumed in natural precipitation over the target area. There is potentially no precipitation augmentation potential. If $T_a \geq T_b$, then $\rho \geq 1$, and natural precipitation processes can be said to be slow. All supercooled liquid water is not consumed in natural precipitation over the target area and an excess is available for conversion to precipitation by cloud seeding. Cloud seeding could induce the excess supercooled liquid water to fall to the surface in the target area.

The timescales ratio brings an added dimension of understanding of supercooled liquid water consumption and precipitation augmentation opportunities beyond the previous interest in E/P of those referenced in section 3b.

d. *Fractional potential precipitation increase* σ

It is useful to relate π and ρ to the *fractional* potential precipitation increase σ that may result from seeding of the observed clouds having the observed precipitation. Here, σ is given by $\sigma = \pi/P$. Given (3c) and (4), we obtain

$$\max(\rho - 1, 0) \leq \sigma \leq \rho. \qquad (5a)$$

Particular cases are

$$\rho - 1 \leq \sigma \leq \rho, \quad \rho \geq 1, \qquad (5b)$$

$$0 \leq \sigma \leq \rho, \quad \rho \leq 1. \qquad (5c)$$

The lower and upper bounds on σ are known as σ_l and σ_u, respectively.

Practical use of (5) requires timely knowledge of the radiometric supercooled liquid water W and the mean precipitation $\bar{r}$ in the cloud seeding target area, and the mean wind speed $\bar{V}$ in the cloudy layer containing the supercooled liquid water and geographic information A and $\bar{d}$. Then, ρ is calculated from this information and substituted into (5) to establish the bounds on σ. With local experience as to how these bounds vary, during prefrontal, frontal, and postfrontal stages of a storm, for example, one can decide when to seed clouds. Of course, the calculated bounds on σ are not a guarantee of achieving the range in (5) of fractional increase in precipitation from seeding because of inefficiencies of the seeding material delivery process and inefficiencies

of the precipitation development and fallout into the target area. Rather, the bounds are illustrative of what might be attempted.

4. Evaluation of water substance variables

This section discusses, for three winter storms, the lower and upper bounds on the precipitation augmentation potential, and the lower and upper bounds on the fractional potential precipitation increase. Reference is made to Table 1, which contains these water substance variables.

The four variables come from 15-min time series of E and P calculated as in (1) and (2). From each time series, a median value of E and P, denoted by $\hat{E}$ and $\hat{P}$, has been calculated for each of several stages of a storm. A median, instead of mean, value reduced the effect of a few extreme values. Then, $\hat{E}$ and $\hat{P}$ were substituted for E and P in (3) and (4) to yield π_l, π_u, and ρ. The values obtained for ρ were substituted in (5) to yield σ_l and σ_u.

Also present in Table 1 for each storm stage is the cloud-top temperature (CTT) (°C), taken from a graph of dewpoint depression versus time and altitude. The adjacent column shows the wind direction in the layer containing the supercooled liquid water as found in Long and Huggins (1992).

The following discussion will treat storms 1, 2, and 3 in turn and search for similarities and differences in water substance variables depending on whether the storm stage was prefrontal, frontal, or postfrontal.

In storm 1 the lower bound on the precipitation augmentation potential π_l increased from prefrontal to frontal to postfrontal stages. A similar behavior was found for the upper bound π_u except that the frontal upper bound was marginally larger than the postfrontal upper bound. There was a similar trend with both the lower and upper bounds of the fractional potential precipitation increase. The storm 1 tabulation of σ_l and σ_u is particularly interesting since it suggests a rather large potential increase of 4.3 (mean of σ_l and σ_u for the first postfrontal stage) and 5.9 (for the second postfrontal stage). (The means are taken to counter the effect of extremes.) Moreover, the precipitation augmentation potential was bounded from 1.8 mm h^{-1} (880 ML h^{-1}) to 2.4 mm h^{-1} (1150 ML h^{-1}) in the postfrontal stages. These were clearly the times to seed.

In storm 2, the bounds on the precipitation augmentation potential for the prefrontal stage were rather similar to the results for the interfrontal and postfrontal stages, suggesting a similarity in supercooled liquid water and precipitation development. Of the two frontal stages, π_l and π_u in the first stage were relatively small, but the second was rather similar to stage 2 of storm 1. The interstorm and intrastorm variations that are observed in storms 1 and 2 in the prefrontal and frontal stages suggest that there is not a uniformity in the precipitation augmentation potentials in these parts of storms. There is more uniformity in the interfrontal and postfrontal stages of storm 2, which have values for π_l and π_u similar to those of storm 1. The fractional potential precipitation increase bounds σ_l and σ_u in the storm 2 interfrontal and postfrontal stages average to 4.4 and 3.0 and are similar to those of storm 1.

In storm 3, both the prefrontal and frontal stages displayed little supercooled liquid water and precipitation development, with π_l and π_u being small. The two postfrontal stages had moderate but somewhat lower values

TABLE 1. Water substance and other variables for three storms.

Storm stage	π_l (ML h^{-1})	π_u (ML h^{-1})	σ_l	σ_u	CTT (°C)	Wind direction (°)
Storm 1						
1—prefrontal	0	150	0	0.79	−30	292
2—frontal	320	1240	0.35	1.35	−22	291
3—postfrontal	880	1110	3.8	4.8	−15	262
4—postfrontal	970	1150	5.4	6.4	−5	242
Storm 2						
1—prefrontal	630	880	2.5	3.5	−45	305
2—frontal	0	120	0	0.14	−45	298
3—interfrontal	550	690	3.9	4.9	−12	238
4—frontal	690	1240	1.3	2.3	−35	235
5—postfrontal	670	940	2.5	3.5	−10	212
Storm 3						
1—prefrontal	0	120	0	0.6	−30	315
2—frontal	0	50	0	0.07	−30	290
3—postfrontal	420	660	1.8	2.8	−20	225
4—postfrontal	430	570	3.1	4.1	−8	240

TABLE 2. Water substance variables for orographic cloud and precipitation bands.

		Orographic cloud				Precipitation band			
Storm	Stages	π_l	π_u	σ_l	σ_u	π_l	π_u	σ_l	σ_u
1	3 and 4	820	900	10.2	11.2	850	1220	2.3	3.3
2	3 and 5	550	630	6.9	7.9	620	850	2.7	3.7
3	3 and 4	440	520	5.5	6.5	410	680	1.5	2.5

than the storms 1 and 2 postfrontal stages. Overall, the postfrontal stages of all three storms were more alike than the prefrontal or the frontal stages were alike. The means of σ_l and σ_u were quite small in the prefrontal and frontal stages but were 2.3 and 3.6 in the postfrontal stages.

With the shallow moist postfrontal flow perpendicular to Baw Baw Plateau, the timescales ratio ρ $(=\sigma_u)$ averaged 4.4 over the three storms. This indicated nonconsumption of most of the supercooled liquid water in its travel and duration above the target area and a significant seeding opportunity. The mean precipitation augmentation potential $[(\pi_l + \pi_u)/2]$ averaged over all three storms was 750 ML h^{-1}, or 1.5 mm h^{-1}, equivalently.

With a deep prefrontal and frontal flow parallel to Baw Baw Plateau, the timescales ratio ρ $(=\sigma_u)$ averaged 1.2, indicative of very rapid and almost complete consumption of the supercooled liquid water while it was above the target area and also indicative of much less seeding opportunity than in the postfrontal stages.

The main conclusion at this point is that the postfrontal stages of winter mountain storms present a rather consistent precipitation augmentation potential of perhaps 1.5 mm h^{-1} or a fractional increase, which on averaging σ_l and σ_u is about 3.9, or 390%. Increases of this magnitude indicate the potential results of the seeding process in these clouds.

5. Postfrontal, orographic, and precipitation band water substance variables

During the postfrontal stages of all three storms, the precipitation amounts fell into two categories. There were amounts greater, and often much greater, than 0.25 mm h^{-1} (121.75 ML h^{-1} flux equivalent), which occurred when a mesoscale precipitation band was passing across the target study area. At other times, between the bands, the precipitation was less than 0.25 mm h^{-1}. This occurred when an orographic cloud lay across the study area. Precipitation bands are a common feature of winter synoptic storms. In the particular context of precipitation enhancement, these have been discussed by Huggins et al. (1989), Long et al. (1990), and Sassen et al. (1990).

Table 2 shows the water substance variables for the postfrontal stages of storms 1, 2, and 3. The lower

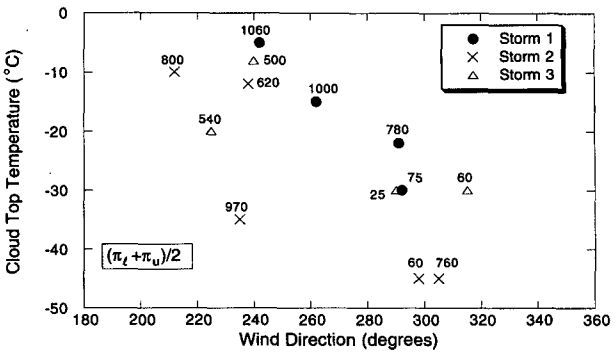

FIG. 3. Relation of mean precipitation augmentation potential $[(\pi_l + \pi_u)/2]$ to cloud-top temperature and wind direction in supercooled liquid water layer for all stages of storms 1, 2, and 3. Each symbol corresponds to one stage of one storm.

bound π_l of the precipitation augmentation potential is about the same for the orographic cloud and precipitation bands, but the upper bound π_u is slightly larger for the precipitation bands. The higher natural base precipitation is also the reason that σ_l and σ_u are smaller for the precipitation bands than for the orographic cloud. Overall, there is a greater precipitation augmentation potential in the precipitation bands averaging 770 ML h^{-1} (1.6 mm h^{-1}), but the average fractional potential precipitation increase is 8.0 in the orographic clouds (as compared to 2.7 in the precipitation bands). Still, both kinds of clouds offer excellent opportunities for precipitation augmentation.

6. Cloud-top temperature and wind direction

The water substance variables in Table 1 depend on the cloud-top temperature and wind direction also tabulated there. Before plotting these variables, we average π_l and π_u, and σ_l and σ_u. The averages are then plotted in Figs. 3 and 4 at the positions of the corresponding cloud-top temperature and wind direction. Figure 3 shows some separation of the average precip-

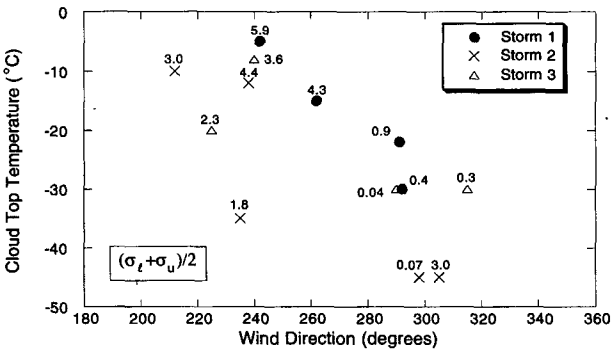

FIG. 4. Same as Fig. 3 but for mean fractional potential precipitation increase $[(\sigma_l + \sigma_u)/2]$.

itation augmentation potential into two higher and lower groups separated by the −20°C temperature line and 260° wind direction line. There are still some higher values of the average, namely 970, 760, and 780 ML h^{-1} in the lower group. This indicates some lack of precision in using cloud-top temperature and wind direction to predict $(\pi_l + \pi_u)/2$.

Figure 4 shows a better separation of the average fractional potential precipitation increase. The same −20°C temperature line and 260° wind direction line are used for delineating the two groups, and only the frontal point labeled 1.8 is not classified. Postfrontal versus frontal-plus-prefrontal storm stages are classified by the −20°C temperature line and 260° wind direction line (see Fig. 5). The postfrontal stages fall within the upper left group, and except for one point, the prefrontal and frontal stages fall within the lower right group.

The dependencies of $(\pi_l + \pi_u)/2$ and $(\sigma_l + \sigma_u)/2$ on both cloud-top temperature and wind direction in Figs. 3 and 4 result from the inverse relation of cloud-top temperature to wind direction. For example, at a wind direction of 240° the cloud-top temperature is about −12°C, while at 300° the temperature is about −35°C. As noted, the wind direction of 240° occurs in postfrontal stages, but it is also important to note that this wind direction is dynamically important for liquid water formation because it results in lift and condensation over the main southwestern face of Baw Baw Plateau. The cloud-top temperature of −12°C also occurs in postfrontal stages and is microphysically important because it is warm and results in a natural reduction in ice production in the clouds. With the 300° direction characteristic of prefrontal and frontal stages, the wind faces the narrow aspect of the plateau, and the orographic component of upward lift is less. Though there can be significant liquid water with any existing frontal component of the lift, the cold cloud-top temperature of −35°C, characteristic of these stages, is conducive to natural ice production.

It is clear then that both the dynamical and microphysical features of the winter storms considered here were responsible for the evolving supercooled liquid water and precipitation fluxes, and, thus, the precipitation augmentation potential and fractional potential precipitation increase in Australian winter mountain storms.

7. Conclusions

The cloud seeding potential of three winter storms in the Great Dividing Range of Australia has been described.

The lower and upper bounds on the precipitation augmentation potential and the fractional potential precipitation increase have been calculated from radiometric liquid water, Omegasonde wind speed, and gauge precipitation data. Averages of the lower and upper

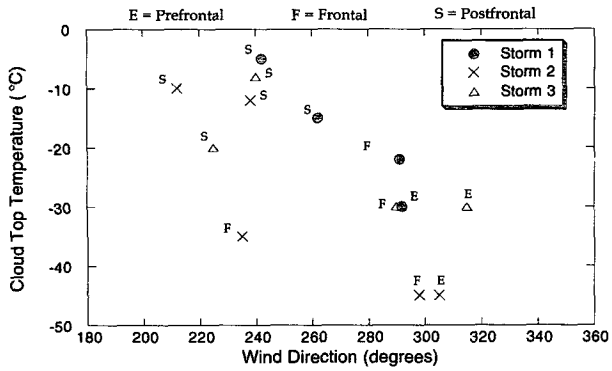

FIG. 5. Prefrontal (E), frontal (F), interfrontal (I), and postfrontal (S) identification of each storm stage cloud-top temperature and wind directions pair.

bounds have been calculated. The results for the fractional potential precipitation increase, considering all storms, are

prefrontal	$(\sigma_l + \sigma_u)/2$	1.2,
frontal	$(\sigma_l + \sigma_u)/2$	0.7,
postfrontal	$(\sigma_l + \sigma_u)/2$	3.9.

These results suggest an opportunity for precipitation augmentation in postfrontal stages.

It should be noted that these figures are considerably larger than the 0.3–0.4 realized by cloud seeding in Tasmania. Clouds clearly offer more of an opportunity for augmentation than obtained with seeding to date.

The three-storm average of the lower and upper bounds of the precipitation augmentation potential π was 750 ML h^{-1} (1.5 mm h^{-1}) in postfrontal stages, including both orographic clouds and mesoscale precipitation bands. This rate occurred over 107 h, and it amounted to a significant 160 mm of potential precipitation.

It is worthwhile to delineate the complement of instrumentation that would be used in a state-of-the-art precipitation augmentation experiment on winter clouds over a mountainous target area. Synoptic weather data would provide the advance warning of a synoptic system. Its presence and structure a few hours ahead of the target area would come from visible and infrared satellite cloud imagery. The imagery would reveal orographic clouds, mesoscale bands, and the main frontal cloud band. A radar of intermediate wavelength (C band) with Doppler and dual-polarization capability would provide details of the clouds. The radar would be carefully located to permit wide scanning angles and to avoid the effects of ground clutter. The Doppler capability would reveal winds that would be supplemented with rawinsonde kinematics information. The dual polarization capability would reveal the kinds of hydrometeors in various parts of the clouds. The sondes

would be particularly important for thermodynamic information on the evolving structure of the atmosphere. All of these sources would provide information on the impending development of clouds to be seeded. As development proceeds, the microwave radiometer supercooled liquid water measurements will come to the fore.

Combination of the radiometer measurements with the Doppler radar and rawinsonde winds would yield E, the supercooled liquid water flux. Real-time precipitation data telemetered from gauges or estimated from the radar would yield the precipitation flux P. This knowledge of E and P would provide the lower and upper bounds on the precipitation augmentation potential π and the timescales ratio ρ. The ratio ρ would be used to place bounds σ_l and σ_u on the fractional potential precipitation increase. The bounds on π and σ would be used to identify clouds susceptible to seeding. These clouds could then be treated.

It should be noted that an instrumented aircraft could be used to measure microphysical cloud properties, such as liquid water and hydrometeors, and supplement the above information. The collective data from the aircraft and other sources could be used to understand and estimate the effect of natural limitations on the cloud seeding process that might reduce the fractional potential precipitation increases.

Acknowledgments. A number of individuals assisted with this work.

At the CSIRO Division of Atmospheric Research (DAR), Ronald Hill and Reg Henry provided logistics support with the remote sensing instrumentation and precipitation gauges. Sunhee Lee provided computer processing of the radiometer, Omegasonde, and precipitation data. Sean Higgins and Louise Carr produced the graphics.

At Melbourne Water (MW), Robert Dorrat was the primary liaison between the MW and the DAR. Ian Searle, John Barry-Murphy, and Peter Murphy provided weather information from the MW cloud seeding experiment. Levente Szirom provided precipitation data from the MW experiment.

At the Bureau of Meteorology, Graham Duff, Colin Irvine, and Julie Matthews operated the Omegasonde equipment and provided processed data.

Richard Smith and Arlen Huggins of the Desert Research Institute installed and operated the microwave radiometer. They also obtained the precipitation microphysics data. Gary Weller prepared the figures.

Toyota provided four-wheel-drive vehicles, and Qantas provided airfares between the United States and Australia.

This research was supported in part by Melbourne Water and in part by the U.S. National Science Foundation Division of Atmospheric Sciences under Grants ATM-8603089, ATM-8812302, and ATM-9108375.

REFERENCES

Boe, B. A., and A. B. Super, 1986: Wintertime characteristics of supercooled liquid water over the Grand Mesa of western Colorado. *J. Wea. Mod.*, **18,** 102–107.

Cooper, W. A., and C. P. R. Saunders, 1980: Winter storms over the San Juan Mountains. Part II: Microphysical processes. *J. Appl. Meteor.*, **19,** 927–941.

Heggli, M., 1986: A ground-based approach used to determine cloud seeding opportunity. Preprints, *Tenth Conf. on Weather Modification,* Arlington, VA, Amer. Meteor. Soc., 64–67.

——, and R. M. Rauber, 1988: The characteristics and evolution of supercooled water in wintertime storms over the Sierra Nevada: A summary of microwave radiometric measurements taken during the Sierra Cooperative Pilot Project. *J. Appl. Meteor.*, **27,** 989–1015.

Hobbs, P. V., 1978: Organization and structure of clouds and precipitation on the mesoscale and microscale of cyclonic storms. *Rev. Geophys. Space Phys.*, **16,** 741–755.

Hogg, D. C., F. O. Guiraud, J. B. Snider, M. T. Decker, and E. R. Westwater, 1983: A steerable dual-channel microwave radiometer for measurement of water vapor and liquid in the troposphere. *J. Climate Appl. Meteor.*, **22,** 789–806.

Huggins, A. W., A. B. Long, and B. A. Campistron, 1989: The impact of mesoscale precipitation bands on liquid water and precipitation efficiency in a winter mountain storm in Utah. *Fifth WMO Scientific Conf. on Weather Modification and Applied Cloud Physics,* Beijing, China, World Meteorological Organization, 55–58.

Long, A. B., and A. W. Huggins, 1992: Australian Winter Storms Experiment (AWSE) I: Supercooled liquid water and precipitation enhancement opportunities. *J. Appl. Meteor.*, **31,** 1041–1055.

——, B. A. Campistron, and A. W. Huggins, 1990: Investigations of a winter mountain storm in Utah. Part I: Synoptic analysis, mesoscale kinematics, and water release rates. *J. Atmos. Sci.*, **47,** 1302–1322.

Marwitz, J., 1986: A comparison of winter orographic storms over the San Juan Mountains and the Sierra Nevada. *Precipitation Enhancement—A Scientific Challenge, Meteor. Monogr.,* No. 43, Amer. Meteor. Soc., 109–113.

Rauber, R. M., and L. O. Grant, 1987: Supercooled liquid water of a shallow orographic cloud system in southern Utah. *J. Appl. Meteor.*, **26,** 208–215.

Sassen, K., A. W. Huggins, A. B. Long, J. B. Snider, and R. J. Meitin, 1990: Investigations of a winter mountain storm in Utah. Part II: Mesoscale structure, supercooled liquid water development, and precipitation processes. *J. Atmos. Sci.*, **47,** 1323–1350.

Super, A. B., and B. A. Boe, 1988: Wintertime cloud liquid water observations over the Mogollon Rim of Arizona. *J. Wea. Mod.*, **20,** 1–8.